

Efficient Simulation of Large Irregular Arrays on a Finite Ground Plane

Jean Cavillot¹, *Student Member, IEEE*, Denis Tihon², *Member, IEEE*, Francisco Mesa³, *Fellow, IEEE*, Eloy de Lera Acedo⁴, and Christophe Craeye¹, *Student Member, IEEE*

Abstract—An efficient method is presented to take into account the radiation pattern deformation due to the presence of a finite ground plane lying under an antenna array and above a layered dielectric medium. The interactions between the antennas and the ground plane are computed using two main algorithms: on one hand, the near-field interactions are carried out using inhomogeneous plane waves, and on the other hand, a new formulation based on an analytical Hankel transform is derived to handle the intermediate-field interactions. This formulation expresses the electric field as a finite series of Hankel functions and associated Anger–Weber functions. The method is validated here for the second version of the square kilometer array (SKA) log-periodic Antenna (SKALA2) and then applied to an SKA low-frequency station (SKA1-LOW).

Index Terms—Anger–Weber functions, FEKO, Green’s function, inhomogeneous plane waves, method of moments (MoM), square kilometer array (SKA).

I. INTRODUCTION

MANY applications involve a large array of antennas above a ground plane. In some of these, the ground plane cannot be considered as infinite but still appears as an electrically large object. In this case, the method of images does not yield an accurate estimate of the impact of the ground plane on the radiation pattern of the array. For example, let us consider the low-frequency antenna of the square kilometer array (SKA) radiotelescope [1], [2] (see Fig. 1) on a finite ground plane of 8 m in diameter. The antenna is positioned at $(x, y) = (-2 \text{ m}, 0 \text{ m})$, off-centered to highlight the broken symmetry of the radiation pattern. The radiation patterns obtained using the method of images are compared in Fig. 2 to those where the finiteness of the ground plane is taken into account using the method presented and validated in [3]. One can see that the patterns are rather different and that the difference is more significant at low frequencies (up to 2 dB within 60° from broadside). This makes it clear that the finiteness of the ground plane has to be included using, for

Manuscript received June 5, 2019; revised September 13, 2019; accepted October 26, 2019. Date of publication November 28, 2019; date of current version April 7, 2020. This work was supported by the Fonds pour la formation à la Recherche dans l’Industrie et l’Agriculture (FRIA) Grant from the Belgium Fonds National de la Recherche Scientifique (FNRS). (*Corresponding author: Jean Cavillot.*)

J. Cavillot and C. Craeye are with ICTEAM, Université catholique de Louvain, 1348 Louvain-la-Neuve, Belgium (e-mail: jean.cavillot@uclouvain.be).

D. Tihon and E. de Lera Acedo are with the Cavendish Laboratory, University of Cambridge, Cambridge CB3 0HE, U.K.

F. Mesa is with the Departamento de Física Aplicada 1, Universidad de Sevilla, 41012 Sevilla, Spain.

Color versions of one or more of the figures in this article are available online at <http://ieeexplore.ieee.org>.

Digital Object Identifier 10.1109/TAP.2019.2955180

0018-926X © 2019 IEEE. Personal use is permitted, but republication/redistribution requires IEEE permission. See <https://www.ieee.org/publications/rights/index.html> for more information.

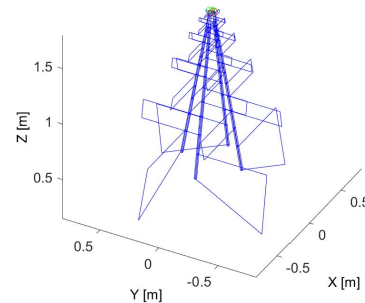


Fig. 1. Second version of the SKA log-periodic antenna (SKALA2) [2].

instance, asymptotic techniques [4], [5] or full-wave simulations [6] employing, for example, the integral equation (IE) methods.

IE methods have proved reliable for the accurate estimation of the electromagnetic properties of antenna arrays and also for the effect of complex platforms. The method of moments (MoM) [7] is often used to solve these equations. However, the complexities of the impedance matrix filling and the Gaussian elimination solution advise against the direct use of this method for large arrays. This issue has been tackled for decades and two categories of methods have been proposed. The first one is based on iterative techniques such as the fast multipole method (FMM) [8] and its multilevel version known as the multilevel fast multipole algorithm (MLFMA) [9]. These methods need a new simulation every time the excitation changes and can suffer from condition-number issues due to fine-mesh details. Additionally, an uncertainty remains regarding the number of iterations needed. The other category of methods corresponds to non-iterative solvers. Among these methods, we find the macro basis function (MBF) method [10], characteristic basis functions (CBFs) [11], synthetic function expansion (SFX) [12], and the entire/sub-entire-domain (SED) basis functions [13]. These methods are based on the assumption that the total current distribution on the antennas can be decomposed into a limited number of current distributions. An advantage of the non-iterative techniques based on MBFs is that the embedded element patterns (EEPs) can be efficiently calculated once the interactions between MBFs have been described, compared to methods based on multilevel fast multipole and its hybridization [14] where a new series of iterations is required for each EEP. Over the last decade, MBFs have become a useful tool to compute the mutual coupling between antennas in large irregular arrays. The MBFs can be constructed, for instance, using plane wave excitations [15], sources on an equivalence

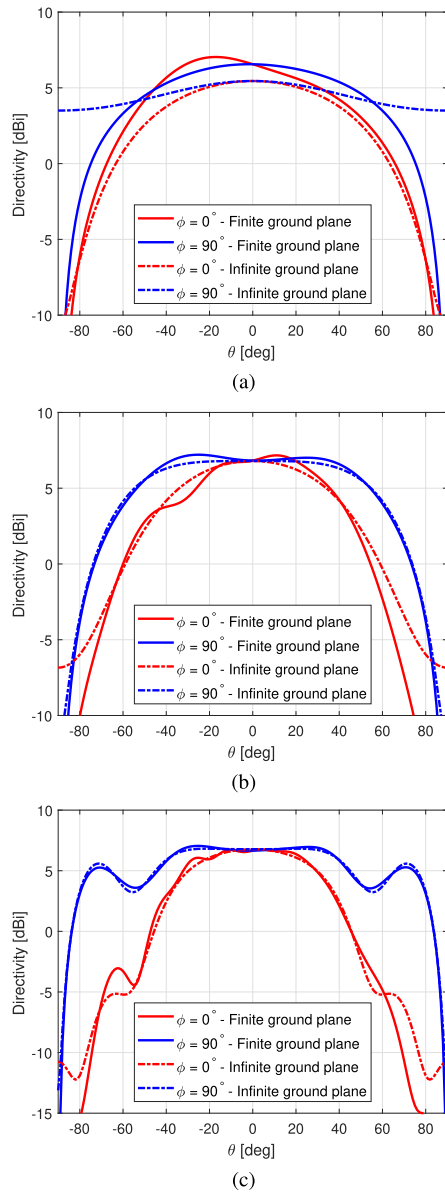


Fig. 2. H-plane ($\phi = 0^\circ$) and E-plane ($\phi = 90^\circ$) radiation patterns of the SKALA2 above an 8 m radius ground plane on semi-infinite dielectric medium of permittivity $\epsilon = 4.8$ at (a) 50 MHz, (b) 110 MHz, and (c) 200 MHz, versus infinite ground plane.

surface [16], or primary and secondary sources [17]. The use of MBFs leads to much smaller systems of equations and fast methods have been developed [18]–[20] to speed up the calculation of the interactions between MBFs. Nevertheless, when considering an electrically large finite ground plane, the interactions between the latter and the MBFs rapidly become prohibitive. That is the problem addressed in this article: the extension of MBF-based methods from arrays problem (for which MBFs are particularly well suited) to the accurate analysis of arrays located on realistic finite ground platforms. In this article, we consider the infinite ground plane solution for the currents on the antennas and then we focus on the interactions between antennas and the finite ground plane. More precisely, the solution on the antennas is computed using MBFs on an infinite ground plane. After that, the goal consists

of speeding up the calculation of fields radiated by MBFs on the antennas and projected on testing functions on the finite ground plane. Two complementary approaches will be used for near-field (up to about one wavelength) and intermediate-field distances. Near-field interactions are computed with inhomogeneous plane waves [21], as briefly initiated in [3]. Such a decomposition combines well with MBF representation of source currents and the number of plane waves remains limited at small lateral distances (measured parallel to the ground plane). However, the efficiency of that approach falls off as the ground plane becomes electrically large. For interactions at intermediate distances (larger than one wavelength), a formulation based on an analytical Sommerfeld Integral (SI) is employed (see background in Appendix A). First, a Fourier series decomposition of the MBF radiation pattern is applied to separate the radial wavenumber and azimuthal dependencies, providing the result as a sum of Hankel transforms. The rational function fitting method (RFFM) [22] is then used to rapidly obtain an accurate estimate of the spatial electric field radiated by an MBF. The formulation leads to an electric field decomposed into cylindrical waves, expressed with a combination of Hankel functions and associated Anger–Weber functions [23]. After that, considering the same set of MBFs for every antenna, the electric field is projected on regularly spaced sampling points of the finite ground plane for each MBFs. Those tables can be reused for each antenna considered as a source. The electric field radiated by all antennas is then integrated on testing functions, providing an excitation vector for the ground plane. The MoM system of equations is finally solved for the ground plane to obtain the equivalent currents. The formulation is very efficient for the analysis of large antenna arrays located over a large finite ground plane.

The remainder of this article is organized as follows. Section II states the mathematical definitions and gives the electric field radiated by an MBF using inhomogeneous plane waves decomposition. The analytical form of the interactions between a given MBF and observation domains is derived for the intermediate field in Section III. Section IV explains how the methods described in Sections II and III are combined with the MoM to obtain the ground plane equivalent currents and acceleration tools based on the symmetry of the ground plane are also described. The proposed approach is then applied and validated to the SKA [1], [2] low-frequency array lying on a finite circular ground plane above a semi-infinite dielectric medium and the simulation time is evaluated. Conclusion is drawn in Section VI.

II. INHOMOGENEOUS PLANE WAVES RADIATED BY MBFs

This section recalls the mathematical framework for the decomposition of the electromagnetic fields into plane waves and for the MBF approach used in this article. The expression of the field radiated by an MBF in terms of inhomogeneous plane waves is then derived.

The fields are decomposed into plane waves using the following conventions:

$$\vec{E} = (-\hat{\mathbf{m}} A_{TE} + \hat{\mathbf{e}} A_{TM}) e^{-jk_x x} e^{-jk_y y} e^{\pm jk_z z} \quad (1)$$

$$\vec{H} = \frac{1}{\eta} (\hat{\mathbf{e}} A_{TE} + \hat{\mathbf{m}} A_{TM}) e^{-jk_x x} e^{-jk_y y} e^{\pm jk_z z} \quad (2)$$

where A is the complex amplitude of the plane wave, the \pm sign denotes the propagation in the $\mp z$ -direction, and η is the medium impedance. The wave vector $\vec{k} = (k_x, k_y, k_z)$ satisfies $k_x^2 + k_y^2 + k_z^2 = k^2 = \omega^2 \mu \epsilon$, with k being the wavenumber, and μ and ϵ the permeability and permittivity of the medium, respectively. To satisfy the radiation condition, $\text{Im}\{k_z\} \leq 0$ is imposed. The TE and TM polarization vectors are defined as follows [24]:

$$\hat{\mathbf{m}}^u = \frac{1}{\beta} \begin{bmatrix} -k_y \\ k_x \\ 0 \end{bmatrix} \quad \text{and} \quad \hat{\mathbf{e}}^u = \frac{1}{\beta k} \begin{bmatrix} k_x k_z \\ k_y k_z \\ -\beta^2 \end{bmatrix} \quad (3)$$

for waves propagating in the $+z$ -direction and

$$\hat{\mathbf{m}}^d = \frac{1}{\beta} \begin{bmatrix} -k_y \\ k_x \\ 0 \end{bmatrix} \quad \text{and} \quad \hat{\mathbf{e}}^d = \frac{1}{\beta k} \begin{bmatrix} -k_x k_z \\ -k_y k_z \\ -\beta^2 \end{bmatrix} \quad (4)$$

for wave propagating in the $-z$ -direction. $\vec{\beta} = (k_x, k_y)$ is the transverse (radial) wave vector and $\beta = (k_x^2 + k_y^2)^{1/2}$ (superscripts u and d stand for upward and downward, respectively).

Let us consider the MoM system of equations: $Zi = v$ where Z is the MoM impedance matrix, i is the vector containing the coefficients to be determined, and v is an excitation vector. Both the vectors i and v are composed of subvectors i_m and v_m , where m corresponds to a given antenna. The matrix Z is composed of blocks Z_{mn} corresponding to the interaction between antennas m and n . As shown in [25], the MBF approach allows for the reduction in the size of that system of equations through the introduction of a matrix Q in which each column corresponds to an MBF. In a nutshell, the solution is approximated as $i_m = Q i_m^r$ such that i^r , which contains significantly less unknowns than i , can be obtained with the following reduced system of equations:

$$Z^r v^r = i^r \quad (5)$$

where $Z_{mn}^r = Q^H Z_{mn} Q$ and $v_m^r = Q^H v_m$ with Q^H the transposed conjugate of Q .

In this article, the MBFs are constructed with primary and secondary excitations [17]. The MBF m can be written as

$$\vec{J}_m = \sum_n \kappa_{n,m} \vec{J}_n(\vec{r}') \quad (6)$$

where $\vec{J}_n(\vec{r}')$ is the n th elementary basis function of the antenna and $\kappa_{n,m}$ is the coefficients of the n th basis function corresponding to the MBF m , which is also corresponding to the entry (n, m) of the matrix Q . The solution on a given antenna is obtained by summing all the MBFs weighted by the coefficients contained in i^r . Such decomposition, combined with fast techniques for the interactions between MBFs, are, for instance, exploited in [26] to calculate the EEPs in large arrays placed on the infinite ground plane. We now look for a fast technique to evaluate the field radiated by the MBFs on

the finite ground plane. Denoting by $\vec{E}_{n,m}$ the field incident to the ground plane due to the MBF m on the antenna n , the total incident field can be expressed as

$$\vec{E}_{\text{tot}} = \sum_n \sum_m^{N_m} i_{n,m}^r \vec{E}_{n,m} \quad (7)$$

where N_a is the number of antennas, N_m is the number of MBFs per antenna, and $i_{n,m}^r$ is the coefficient specific to the MBF m and the antenna n . The vector i^r is obtained by solving (5). Note that (7) can be efficiently evaluated if the same set of MBFs is used on each antenna.

The remainder of the section is devoted to the evaluation of the field radiated by a given MBF using inhomogeneous plane waves. Algorithms based on inhomogeneous plane waves have been extensively used recently to compute the field radiated by a given current distribution and tested by another distribution. It allows for the reduction in the complexity of the interactions between subdomains as their distance increases [27]. Error bounds can be derived to determine the minimum number of inhomogeneous plane waves needed for a given problem [28]. Besides, one may benefit from a compensation between aliasing and truncation errors when the integral is performed with rectangles along the steepest descent path (SDP) [29].

Following the derivations shown in Appendix B reading the Green's function as the Weyl integral [30], the spatial electric field radiated below a given MBF in free space (the index m used in (6) will be suppressed) for a given polarization p (TE or TM) can be written as follows:

$$\vec{E}_p(x, y, z) = -\frac{jk\eta}{(2\pi)^2} \iint_{-\infty}^{\infty} \hat{\mathbf{e}}_p F_p(k_x, k_y) \times \frac{e^{-j(k_x x + k_y y - k_z z)}}{2jk_z} dk_x dk_y \quad (8)$$

where

$$F_p(k_x, k_y) = \sum_n \kappa_n \iiint_{V'} \hat{\mathbf{e}}_p \cdot \vec{J}_n(\vec{r}') \times e^{j(k_x x' + k_y y' - k_z z')} dV' \quad (9)$$

is the radiation pattern of the MBF. In the obtaining of (8), it has been taking into account that now

$$\hat{\mathbf{e}}_p \cdot \left[\mathbb{I} - \frac{\vec{k}\vec{k}}{k^2} \right] \cdot \vec{J}_n = \hat{\mathbf{e}}_p \cdot \vec{J}_n \quad (10)$$

In this method, it is necessary to deform the integration path along the radial wavenumber into the complex plane to avoid the singularity lying on the real axis. The path selected for the radial wavenumber $\beta = \beta_R + j\beta_I$ is given as [31]

$$\beta_I = A\beta_R e^{-\frac{\beta_R}{k}} \quad (11)$$

with A a chosen constant. Note that, due to this contour deformation, k_x and k_y will simultaneously include real and imaginary parts, leading to a decomposition into inhomogeneous plane waves. The contour deformation can be rewritten as an integration over real k_x and k_y coordinates, while still respecting (11), as explained in [24] and [32].

In this article, the antenna is standing above a layered dielectric medium. The reflection by the soil can be handled by computing the reflection coefficients [33] and adding their contribution as follows [24]:

$$\vec{E}_p(x, y, z) = \frac{-jk\eta}{(2\pi)^2} \iint F_p(k_x, k_y) \frac{e^{-j(k_x x + k_y y - k_z z)}}{2jk_z} \times [\hat{\mathbf{e}}_p^d + \Gamma_p(\beta)\hat{\mathbf{e}}^u] dk_x dk_y. \quad (12)$$

Let us consider a vertical distance z' and a radial distance ρ between the basis functions of the antennas and the testing functions of the ground plane. The number of inhomogeneous plane waves needed remains limited when the field of view ρ/z' is relatively small [28]. In our application, the antenna's lowest basis functions are relatively close to the ground plane (z' around $\lambda/10$ at the central frequency). In this case, the electric field cannot be efficiently estimated over radial distances larger than about two wavelengths using the inhomogeneous plane waves expansion. Hence, another method is necessary for larger radial distances. Section III is devoted to the development of a new technique to efficiently obtain field projections at larger distances.

III. INTERMEDIATE FIELD

As stated above, the method based on inhomogeneous plane waves loses its efficiency with increasing radial distance between the MBFs and the ground plane testing functions. In this section, we describe the steps leading to a new formulation of the electric field radiated by an MBF. Starting from the double-integral representation in (12), the transverse field radiated on the plane $z = 0$ is re-expressed as a sum of cylindrical waves using Hankel and associated Anger–Weber functions.

First, let us apply a change of coordinates in (12). Defining ρ , ϕ , and α such that $x = \rho \cos \phi$, $y = \rho \sin \phi$, $k_x = \beta \cos \alpha$, and $k_y = \beta \sin \alpha$, the electric is given by

$$E_{p,i}(\rho, \phi) = \frac{-jk\eta}{(2\pi)^2} \int_0^\infty \int_0^{2\pi} e_{p,i}(\beta, \alpha) F_p(\beta, \alpha) \times \tilde{G}_p(\beta) e^{-j\beta\rho \cos(\alpha-\phi)} d\alpha \beta d\beta \quad (13)$$

where the subscript i refers to Cartesian component, x or y , of the field tangential on the ground plane, and

$$\tilde{G}_p(\beta) = \frac{[1 \pm \Gamma_p(\beta)]}{2jk_z}. \quad (14)$$

Thus, the i th component of the total field is the sum of the contributions of TE and TM polarizations: $E_i = E_{TE,i} + E_{TM,i}$. Multilayered media are accounted for through an appropriate reflection coefficient $\Gamma_p(\beta)$, preceded by a sign which depends on the polarization p (+ for TE and – for TM). The rest of the development is similar for any polarization p and coordinate i . From here, a truncated Fourier series of the radiation pattern is used to separate dependencies on the radial wavenumber and on the azimuthal angle

$$e_{p,i}(\beta, \alpha) F_p(\beta, \alpha) = \sum_{n=-N/2}^{N/2} \tilde{K}_n(\beta) e^{jn\alpha} \quad (15)$$

where

$$\tilde{K}_n(\beta) = \frac{1}{2\pi} \int_0^{2\pi} e_{p,i}(\beta, \alpha) F_p(\beta, \alpha) e^{-jn\alpha} d\alpha. \quad (16)$$

Equation (13) then becomes

$$E_{p,i}(\rho, \phi) = \frac{-jk\eta}{(2\pi)^2} \sum_{n=-N/2}^{N/2} \int_0^\infty \tilde{K}_n(\beta) \tilde{G}_p(\beta) \times \int_0^{2\pi} e^{-j\beta\rho \cos(\alpha-\phi)} e^{jn\alpha} d\alpha \beta d\beta \quad (17)$$

where the sum and integration operators have been swapped. Taking into account that the integration with respect to α in (17) can be analytically solved as [34, Sec. 8.41]

$$\int_0^{2\pi} e^{-j\beta\rho \cos(\alpha-\phi)} e^{jn\alpha} d\alpha = -2\pi e^{jn(\phi+3\pi/2)} J_n(\beta\rho) \quad (18)$$

the electric field now reads

$$E_{p,i}(\rho, \phi) = \frac{jk\eta}{2\pi} \sum_{n=-N/2}^{N/2} e^{jn(\phi+3\pi/2)} \times \int_0^\infty \tilde{K}_n(\beta) \tilde{G}_p(\beta) J_n(\beta\rho) \beta d\beta. \quad (19)$$

The electric field is now written as a sum of Hankel transforms which can be rapidly evaluated with the RFFM [22], which consists of writing part of the integrand in a pole-residue form and applying the appropriate integration path. To this end, for every Fourier component n , the product $\tilde{K}_n(\beta)\tilde{G}_p(\beta)$ is approximated as the following finite pole-residue representation:

$$\tilde{K}_n(\beta)\tilde{G}_p(\beta) = \sum_{q=1}^M \frac{a_{q,n}}{\beta^2 - p_{q,n}^2}, \quad n = -N/2, \dots, N/2 \quad (20)$$

where M is the number of residues, and $a_{q,n}$ and $p_{q,n}$ are the amplitude and the position of the poles used to approximate the function, respectively. Those coefficients can be found by solving small system of equations based on total least squares [31] or on the VECTFIT algorithm [35]–[37]. Using this formulation and multiplying the numerators and denominators of (19) by β^{n-1} , the electric field can be written as

$$E_{p,i}(\rho, \phi) = \frac{jk\eta}{2\pi} \sum_{n=-N/2}^{N/2} e^{jn(\phi+3\pi/2)} \int_0^\infty \sum_{q=1}^M \frac{a_{q,n}}{\beta^2 - p_{q,n}^2} \times \frac{1}{\beta^{n-1}} J_n(\beta\rho) \beta^n d\beta. \quad (21)$$

Note that the function $(1/\beta^{n-1}) \sum_{q=1}^M a_{q,n}/(\beta^2 - p_{q,n}^2)$ is even with respect to β when n is odd and, conversely, the function is odd when n is even. This observation will lead to a closed-form expression for (21) through the use of two theorems found in [38] regarding contour integration (see Appendix C). Thanks to those two theorems, the electric

field in (21) can now be expressed as

$$E_{p,i}(\rho, \phi) = \frac{-k\eta}{4} \times \left[\sum_{\substack{n=-N/2 \\ n \text{ even}}}^{N/2} e^{jn(\phi+3\pi/2)} \sum_{q=1}^M a_{q,n} H_n^{(2)}(p_{q,n} \rho) + \sum_{\substack{n=-N/2 \\ n \text{ odd}}}^{N/2} e^{jn(\phi+3\pi/2)} \sum_{q=1}^M a_{q,n} \mathcal{H}_n^+(p_{q,n} \rho) \right] \quad (22)$$

where $H_n^{(2)}$ is the Hankel function of second kind and order n , \mathcal{H}_n^+ is a linear combination of both Anger and Weber functions of order n (see Appendix C), the sign of $p_{q,n} = (p_{q,n}^2)^{1/2}$ is taken such that the radiation conditions are satisfied; i.e., such that $\Im\{p_{q,n}\} < 0$. It is, thus, necessary to efficiently compute the Weber function for negative imaginary arguments (see Appendix C).

To sum up, we first compute the radiation pattern of a given MBF. The double integral in (13) is transformed into a finite sum of single integrals through the use of a truncated Fourier series of the radiation pattern. After that, the RFFM is used to obtain a pole-residue form of the integrand. Finally, a closed-form expression of the electric field (22) radiated by the MBF is obtained thanks to contour integration. This formulation allows us to directly evaluate the intermediate field while keeping only a few poles and residues in memory.

IV. IES AND ACCELERATION

In this section, the MoM is applied to obtain the equivalent currents on the ground plane. A tool based on circulant matrix that accelerates the solution of the MoM system of equations is presented. After that, the radiation patterns of the antennas and ground plane are derived.

Starting from the antenna currents i_a which result of a given excitation (either at the element level to obtain the EEP or at the array level to obtain the array pattern), obtained with an infinite ground plane, the currents i_g on the finite ground plane can be obtained from the following MoM system of equations:

$$\begin{bmatrix} Z_{ga} & Z_{gg} \end{bmatrix} \begin{bmatrix} i_a \\ i_g \end{bmatrix} = \begin{bmatrix} 0_g \end{bmatrix} \quad (23)$$

where $[0_g]$ is a vector containing zeros, Z_{ga} is the matrix corresponding to the interaction between antennas and the ground plane, and Z_{gg} corresponds to the self-interaction of the finite ground plane. In our case, the goal is to efficiently compute $Z_{ga}i_a$. This term is calculated by computing the fields radiated by each of the MBFs, using the methods described in Sections II and III, and then by projecting them on sampling points of the ground plane. More precisely, the field incident to the ground plane is tabulated on a rectangular grid for each MBF. After that, the field radiated by a given antenna is computed as the sum of the fields radiated by each MBF weighted by the MBF coefficients specific to the antenna. The procedure is repeated for each antenna to obtain (7). The total field is then interpolated and integrated on the ground plane

testing functions using a three-point quadrature, thus obtaining $Z_{ga}i_a$. Finally, the MoM system of equations is solved to obtain the ground plane equivalent currents.

Given the configuration of our problem, it is possible to benefit from symmetries and redundancies. For example, the ground plane considered is sectorially symmetrical and can be discretized into identical angular sectors. Let us denote as n_s the number of sectors. From this discretization, the following circulant MoM matrix [39] Z_{gg} is obtained for the basis functions on the ground plane:

$$Z_{gg} = \begin{bmatrix} Z_{11} & Z_{12} & \dots & Z_{1n_s-1} & Z_{1n_s} \\ Z_{1n_s} & Z_{11} & \dots & Z_{1n_s-2} & Z_{1n_s-1} \\ \vdots & \vdots & \ddots & \vdots & \vdots \\ Z_{12} & Z_{13} & \dots & Z_{1n_s} & Z_{11} \end{bmatrix} \quad (24)$$

where Z_{ij} is the interaction between the angular sectors i and j . This property allows us to reduce the matrix filling time by a factor n_s and solve the MoM system of equations by inverting n_s small matrices instead of inverting as a whole Z_{gg} . Let us define $i_g = [i_{g0}^T, i_{g1}^T, \dots, i_{gn_s-1}^T]^T$ the vector containing the solution of each angular sector and $v_g = -Z_{ga}i_a = [v_{g0}^T, v_{g1}^T, \dots, v_{gn_s-1}^T]^T$ the excitation vector resulting from the projection of (7) on the ground plane testing functions. If we define $\tilde{i}_{gn} = \sum_{m=0}^{n_s-1} i_{gm} e^{-jmn2\pi/n_s}$ and $\tilde{v}_{gn} = \sum_{m=0}^{n_s-1} v_{gm} e^{-jmn2\pi/n_s}$, then [39], [40]

$$\text{Diag}\{\tilde{Z}_{11}, \dots, \tilde{Z}_{1n_s}\} \tilde{i}_g = \tilde{v}_g / n_s \quad (25)$$

where $\tilde{Z}_{1n} = \sum_{m=0}^{n_s-1} Z_{1m} e^{jmn2\pi/n_s}$, $\tilde{i}_g = [i_{g0}^T, i_{g1}^T, \dots, i_{gn_s-1}^T]^T$, and $\tilde{v}_g = [v_{g0}^T, v_{g1}^T, \dots, v_{gn_s-1}^T]^T$. After that, the solution can be obtained as $i_{gn} = \sum_{m=0}^{n_s-1} i_{gm} e^{jmn2\pi/n_s}$.

The radiation pattern of combined antennas and ground plane has three main contributions:

- 1) The direct radiation from the antennas;
- 2) The reflection by the soil;
- 3) The contribution of the finite ground plane.

The direct radiation by a given MBF can be computed by simply taking the following radiation integral:

$$F_p(\hat{\mathbf{u}}^+) = \sum_n \kappa_n \iint \tilde{J}_n(\tilde{\mathbf{r}}') \cdot \hat{\mathbf{e}}_p^+ e^{jk\tilde{\mathbf{r}}' \cdot \hat{\mathbf{u}}^+} dS \quad (26)$$

with $\hat{\mathbf{u}}^+ = (k_x, k_y, k_z)/k$ defining the unit vector associated with the direction of a wave propagating with an elevation angle $\theta \in [0, \pi/2]$. The waves reflected by the soil are accounted for by combining the previous equation for waves propagating downward and the reflection coefficient of the soil. The direct radiation of the MBF combined with the reflection by the soil can be written as

$$F_p(\hat{\mathbf{u}}^+) + \Gamma_p F_p(\hat{\mathbf{u}}^-) \quad (27)$$

with $\hat{\mathbf{u}}^- = (k_x, k_y, -k_z)/k$. Note that, if every antenna supports the same set of MBFs, the array pattern can be obtained by combining the radiation pattern of the MBFs with the array factor. The third contribution is the radiation from

the ground plane equivalent currents. The radiation pattern of a given basis function can be computed as follows:

$$\vec{F}_{gp}(\hat{\mathbf{u}}^+) = \frac{-\mathbf{j}}{\lambda}(\hat{\mathbf{u}}^+ \times \hat{\mathbf{z}} \times \vec{f}(k_x, k_y)) \quad (28)$$

and

$$\vec{f}(k_x, k_y) = \vec{\tilde{\mathbf{G}}}(k_x, k_y) \cdot \vec{\tilde{\mathbf{j}}}(k_x, k_y). \quad (29)$$

$\vec{\tilde{\mathbf{G}}}(k_x, k_y)$ being the spectral dyadic Green's function and $\vec{\tilde{\mathbf{j}}}(k_x, k_y)$ the Fourier transform of the Rao–Wilton–Glisson (RWG) basis functions representing the ground plane.

V. APPLICATION TO SKA1-LOW ARRAYS

For validation of the proposed method, we consider arrays devoted to radio astronomy [2]. First, the method will be validated in small arrays in comparison with the commercial software FEKO [41]. After that, the method is applied to the full array and a simulation time evaluation of the algorithm is given. The stations of the low-frequency SKA radio-telescope [1] will be lying on a large finite ground plane and, as the antennas operate at relatively low frequencies (50–350 MHz), these platforms can have a significant impact on the radiation pattern. Due to the ground plane finiteness, the method of images cannot be used and one must study the coupling between the ground plane and the antennas. A software named HARP [26] has been designed to efficiently compute the mutual coupling between the antennas assuming an infinite ground plane. HARP is based on an MBF approach and a technique providing a model for the interactions between MBFs. These MBFs are built using primary and secondary excitations [17] and a current distribution is defined for each of them on the whole antenna. It is found that the antenna currents calculated with HARP constitute a good approximation of the exact solution including the finite ground plane. Considering this approximation, the equivalent currents of the finite ground plane can be obtained with the methods presented in Sections II–IV. The ground plane is meshed here with RWG basis functions [42]. The antenna considered is the second version of the SKA log-periodic antenna (SKALA2) [2] (see Fig. 1), which is meshed here with 1218 linear basis functions. The SKALA2 antenna is a dual-polarized element (X and Y polarization) made of four arms supported by four spines. In this article, only the Y-oriented excitation is considered, and similar results are obtained for excitation at X-arms. Since the ground plane is of finite extent, the coupling of the antenna with the soil has to be taken into account. A picture of the SKALA2 antenna lying on a finite ground plane lying itself on a semi-infinite soil is shown in Fig. 3. Air and soil correspond to media 1 and 2, respectively. The soil relative permittivity is considered $\epsilon_2 = 4.8$. Given that the antenna and the finite ground plane are lying above a semi-infinite dielectric medium, the TE and TM reflection coefficients defined as the ratio between the reflected and incoming waves read [43]

$$\begin{aligned} \Gamma_{\text{TE}}(\beta) &= \frac{ct_1\eta_2 - ct_2\eta_1}{ct_1\eta_2 + ct_2\eta_1} \\ \Gamma_{\text{TM}}(\beta) &= \frac{ct_1\eta_1 - ct_2\eta_2}{ct_1\eta_1 + ct_2\eta_2} \end{aligned} \quad (30)$$

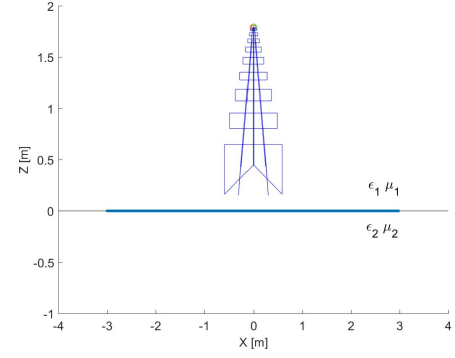


Fig. 3. SKALA2 on a finite ground plane lying itself on an infinite soil.

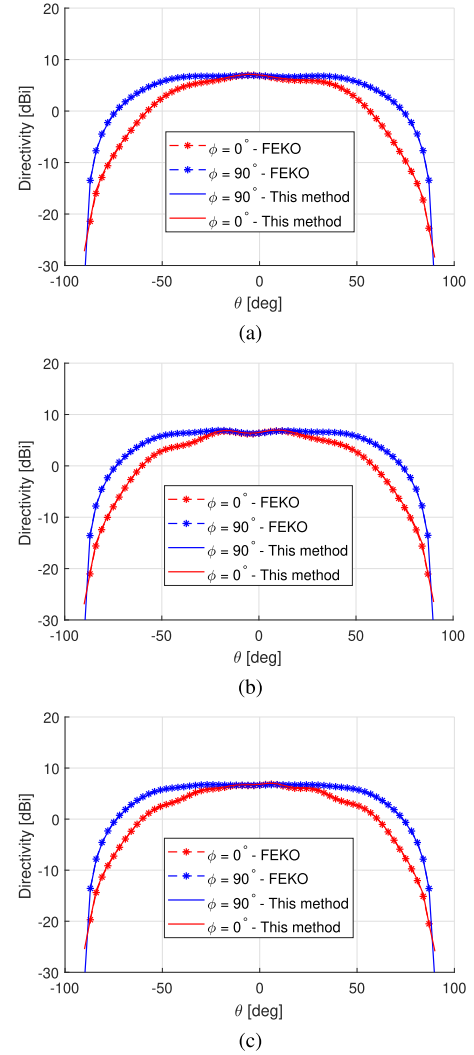


Fig. 4. Radiation pattern of the SKALA2 above (a) 4 m, (b) 6 m, and (c) 8 m, radius ground plane at 110 MHz.

with index 1 referring to the air and index 2 to the soil, and

$$ct_i = \frac{k_{z,i}(\beta)}{k_i}. \quad (31)$$

Let us consider the radiation pattern of an SKALA2 antenna positioned at $(x, y) = (0.5, 0.5)$ m on a circular ground plane centered at $(x, y) = (0, 0)$ of radii 4, 6, and 8 m, displayed in Fig. 4. They have been computed using the presented

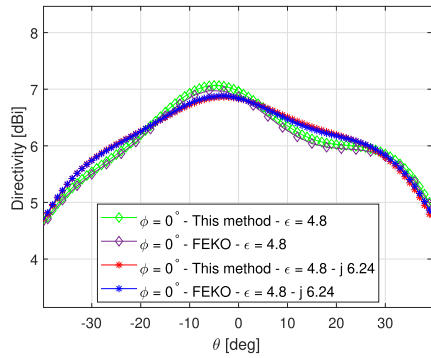


Fig. 5. Radiation pattern of the SKALA2 above a 4 m radius ground plane at 110 MHz, considering both lossless and lossy dielectric media for the soil.

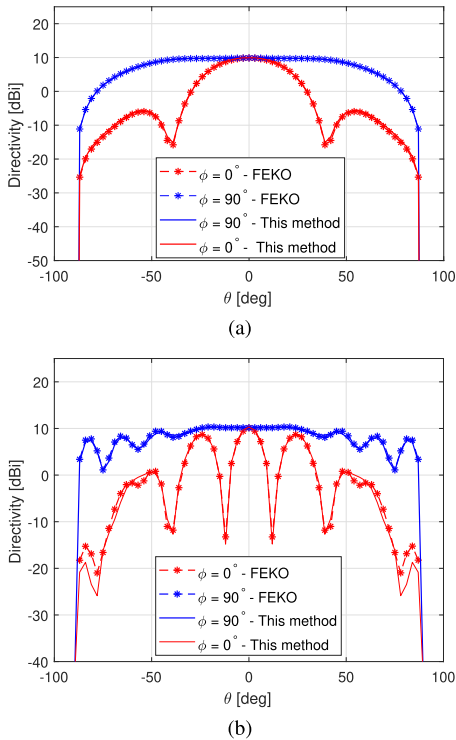


Fig. 6. Radiation pattern of the two antennas above a 4 m radius ground plane at (a) 110 MHz and (b) 350 MHz.

method and compared with the results from the commercial software FEKO [41]. The planes $\phi = 0^\circ$ and $\phi = 90^\circ$ correspond to the H-plane and E-plane, respectively. The simulation results are consistent with those from FEKO. The simulation is also done considering a complex permittivity $\epsilon_2 = 4.8 - j6.24$ for the soil. The results are compared to those of FEKO and to those including a lossless soil in Fig. 5. A difference smaller than 0.1 dB is observed between our results and those of FEKO. Next, we consider two SKALA2 antennas with the first one positioned in $(x_1, y_1) = (1, 0)$ m and the second one in $(x_2, y_2) = (-1, 0)$ m. These antennas lie on a 4 m radius ground plane. The radiation pattern obtained with the proposed method and with FEKO is compared in Fig. 6 at frequencies of 110 and 350 MHz, respectively. The results agree with those of FEKO but differences of the order of 1 to 2 dBs appear in the H-plane sidelobes for the data at 350 MHz. As already stated in [26], those differences could come from

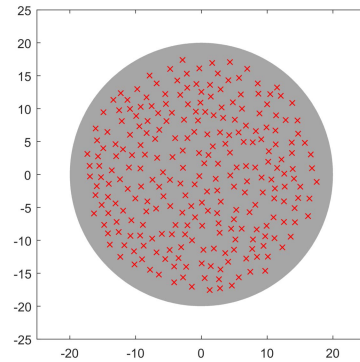


Fig. 7. Configuration of the full SKA low-frequency station lying on a finite ground plane lying itself on infinite soil.

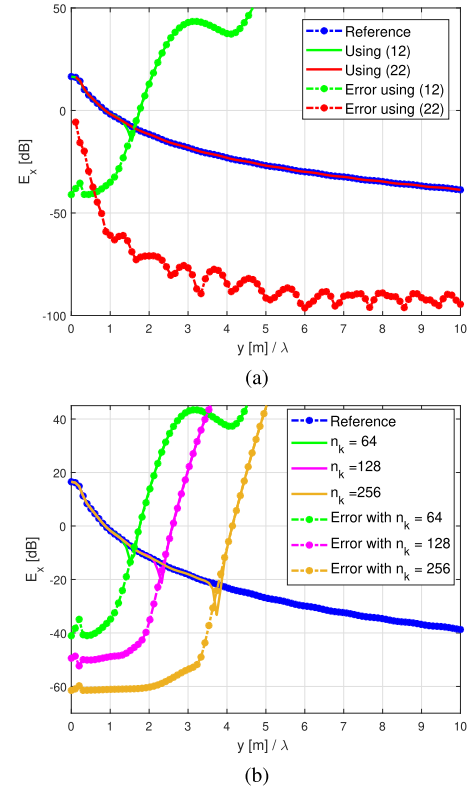


Fig. 8. Component x of the electric field radiated on the ground plane by the SKALA2 antenna at 110 MHz. The field is evaluated along y with $x = 0$. Field computed with (a) (22) and (b) (12).

the differences between our antenna model and the one used in FEKO.

Let us now consider 256 SKALA2 antennas lying on a finite circular ground plane of 40 m diameter, as pictured in Fig. 7. The array is irregular in order to randomize the sidelobes and mutual coupling effects. The frequencies selected here are 50 and 110 MHz. Each antenna is meshed with 1218 linear basis functions and the ground plane is meshed with 34584 RWG basis functions. For the HARP simulation, the final current distribution on the antennas is obtained using 20 MBFs. The interactions between MBFs and the finite ground plane are obtained with the methods described in Sections II and III. The method described in Section II is used for the near-field interactions and the one described in Section III is used for the intermediate-field interactions. The accuracies of these

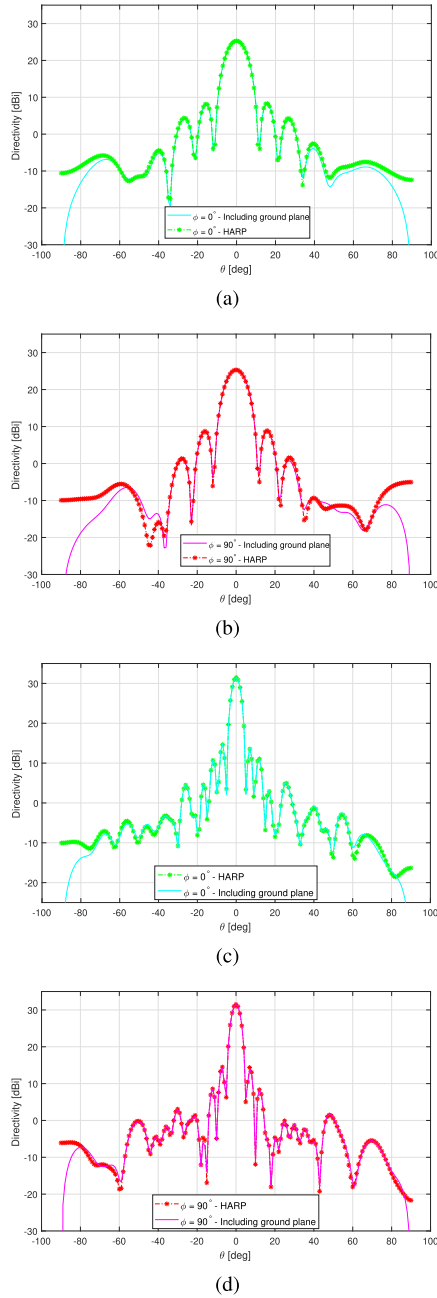


Fig. 9. Radiation pattern of the array at (a) 50 MHz: H-plane cut, (b) 50 MHz: E-plane cut, (c) 110 MHz: H-plane cut, and (d) 110 MHz: E-plane cut.

methods are compared in Fig. 8 (a). In this figure, the reference electric field is obtained with formula (12) using a great number of 2048×2048 inhomogeneous plane waves for which the convergence has been checked. The reference is compared with the solution obtained with formula (12) using 64×64 inhomogeneous plane waves and with formula (22) using $N = 10$ and $M = 12$. In the near-field ($\rho < \lambda$), the accuracy of (22) rapidly deteriorates due to the Hankel functions singularity. In contrast, formula (12) using 64×64 inhomogeneous plane waves provides a fast and good estimation of the electric field for lateral distances $\rho < \lambda$. The error rapidly increases for larger distances due to the increasing oscillations of the integrand [28] and a larger number of integration points is necessary as shown in Fig. 8(b). In this figure, the electric

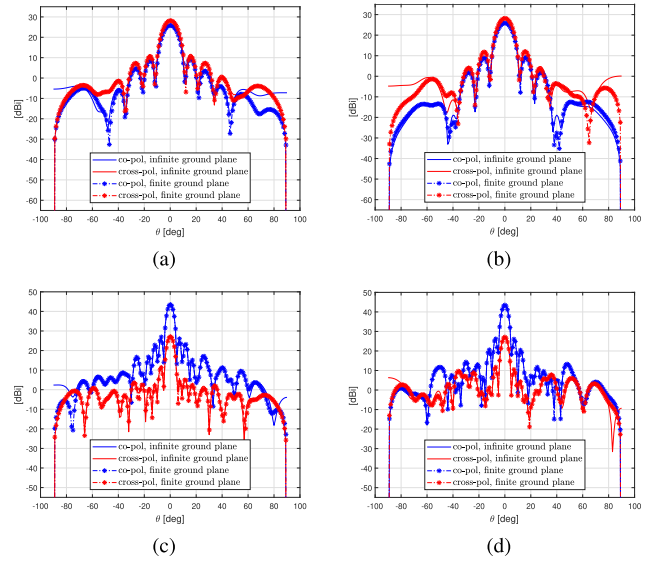


Fig. 10. Cross-polarization and co-polarization of the array at (a) 50 MHz: H-plane cut, (b) 50 MHz: E-plane cut, (c) 110 MHz: H-plane cut, and (d) 110 MHz: E-plane cut.

field is computed with $n_k \times n_k$ inhomogeneous plane waves for different values of n_k . It is shown that the required number of plane waves significantly increases with increasing distance of interaction. The choice of ρ_0 as a transition distance ($\rho_0 = \lambda$ recommended here) from one method to the other may be slightly dependent on the type of antenna. However, we observed a broad range of possible values for ρ_0 (typically from 0.6λ to 2λ), without significant impact on computation time nor accuracy. Here, we choose the inhomogeneous plane waves expansion for $\rho < \lambda$ with formula (12) using 64×64 inhomogeneous plane waves and formula (22) with 11×12 cylindrical waves is used for $\rho \geq \lambda$, where the error is low and stable.

The radiation pattern of the full array made of 256 SKALA2 antennas is displayed in Fig. 9(a)–(d) and compared with the infinite ground plane case. Fig. 9(a) and (b) shows that some important variations can appear at low frequencies for elevation angles greater than 35° . The simulation shows that the ground plane finiteness is not of great concern for the SKA1-low full station radiation pattern at 110 MHz. Nevertheless, 1 dB variations can appear for elevation angles greater than 60° . More information about the possible impact of sidelobes on the performance of the SKA-low station can be found in [44]. The plots in Fig. 10 compare the co- and cross-polarization levels for the infinite ground plane and finite ground plane cases. Those patterns are obtained using the Ludwig-3 definition [45]. As observed and discussed in [46], it appears that the cross-polarization pattern is about 2 dB higher than the co-polarization pattern in the main beam at low frequency. This high cross-pol level does not prevent accurate polarization estimation when both arms of each antenna are used, as explained in [47]. At 110 MHz, the co-polarization pattern is about 15 dB higher than the cross-polarization pattern in the main beam.

The method presented here is performed after getting the infinite ground plane solution from the HARP software [26].

TABLE I
TIME EVALUATION OF THE PROPOSED METHOD AT 110 MHz

Step	Required Time
Computation of poles, residues for (22)	15 sec / MBF
Tabulation of the field radiated by every MBF on large rectangular grids using (12) and (22)	30 sec/MBF
Pre-computation of the Fourier transform of the currents on one angular sector of the ground plane for (29)	90 sec
Ground plane meshing and calculation of Z_{gg}	50 min
Direct and reflected radiation using the array factor with (27)	40 sec
Interpolate and project the electric field on the ground plane	25 sec/MBF
Solve the MoM system of equations for the ground plane	2 min
Compute the radiation of the ground plane equivalent currents	1 sec

At a given frequency, the software HARP needs 3 h of preprocessing and then the array can be simulated on infinite ground plane for any configuration of the antennas positions. The simulation time of HARP is compared to those of different commercial softwares in [26]. An evaluation of the time required by the method proposed in this article is given in Table I. The simulation is carried out using a single computer equipped with an Intel Core i5-7500 CPU with a 3.4 GHz clock and 24 GB of RAM. The software is written in MATLAB language, release R2017a, along with some C++ routines for the fast calculation of the ground plane MoM matrix. Note that the first two steps in Table I are independent of the ground plane and array configurations and must be carried out only once for each frequency. Only the last four steps need to be executed again if the position of the antennas or the excitation port are modified (assuming the new infinite ground plane solution on the antennas from the HARP software). In this simulation, the radiation pattern is obtained for 120 azimuthal angles \times 91 elevation angles. Note that the ground plane radiation pattern can be obtained from (29) by computing the Fourier transform of the equivalent currents of one angular sector. Indeed, the contribution from the other sectors can be obtained by rotating and adding their radiation patterns. The interactions between antennas and the ground plane have been accelerated and most of the simulation time is now allocated to the calculation of the ground plane MoM matrix, as shown in Table I.

VI. CONCLUSION

The numerical analysis of finite antenna arrays has known tremendous acceleration over the past two decades, among others based on MBF representations. We tackled here the challenge of the interaction with the near-field environment through the analysis of scattering by the edges of the ground plane underlying the array. In this article, an efficient method for the fast and accurate calculation of scattering by a finite ground plane lying under irregular antenna arrays is presented. The method is based on the efficient calculation of the interactions between MBFs and the finite ground plane. The interactions are carried out using algorithms based on

inhomogeneous plane waves in the near field and a new formulation using Hankel and Anger–Weber functions is used for the intermediate-field interactions. Moreover, the method can be accelerated using circulant matrix for the finite ground plane self-interaction. For applications such as the SKA [1], this method provides higher accuracy for the EEP involved in the calibration stage.

APPENDIX A ANALYTICAL SI BACKGROUND

In the MoM [7], an essential step is the computation of SIs to determine the spatial Green's functions. Solving these infinite integrals is a time-consuming process due to their oscillating and slowly decaying behavior. The problem has been tackled for decades and a great variety of solutions exist today. Some techniques involve the Fast Hankel Transform [48], the window function approach [49], or the integration along the Sommerfeld integration path (SIP) with the integration on the real axis accelerated through the partition-extrapolation method [50]. Among those methods, the most popular ones are the discrete complex image method (DCIM) [51] and the RFFM [22]. Both methods are able to give simple forms of the SIs for a great range of distances between the source and observation domains. The DCIM gives the solution as a sum of spherical waves but requires the analytical extraction of cylindrical surface wave terms for far-field estimation. Indeed, the far-field near the substrate is often dominated by those cylindrical waves. The RFFM, however, directly describes the result as a sum of cylindrical waves as a finite series of Hankel functions. The RFFM, in contrast to the DCIM, fails to give an accurate estimation in the near field due to the non-physical singularity exhibited by the Hankel functions when the source and the observation points do not lie in the same plane. In [31], the RFFM is improved to solve the Hankel function singularity problem.

APPENDIX B ELECTRIC FIELD IN FREE SPACE

The derivation provided here is similar to the one given in [24] and [27]. Let us consider the free-space Green's function expressed as the Weyl integral [30]

$$\begin{aligned}
 G(R) &= \frac{e^{-jkR}}{4\pi R} \\
 &= \frac{1}{(2\pi)^2} \iint_{-\infty}^{+\infty} \tilde{G}(k_x, k_y) e^{-j[k_x(x-x') + k_y(y-y')]} \\
 &\quad \times dk_x dk_y
 \end{aligned} \tag{32}$$

where $R = |\vec{r} - \vec{r}'|$, $\vec{r}' = (x', y', z')$ is the source coordinates, and $\vec{r} = (x, y, z)$ the observation coordinates. The spectral Green's function is given by

$$\tilde{G}(k_x, k_y) = \frac{e^{-jk_z|z-z'|}}{2jk_z} \tag{33}$$

with $k_x^2 + k_y^2 + k_z^2 = k^2$. The vector potential in free space due to electric current density \vec{J}_b can be expressed as

$$\vec{A}(x, y, z) = \iiint_V G(R) \vec{J}_b(x', y', z') dV' \tag{34}$$

where V' is the volume enclosing the source. The spatial electric field can be expressed as the summation of the inverse Fourier transforms of both the TE and TM spectral electric fields

$$\begin{aligned}\vec{E}(x, y, z) &= \vec{E}_{\text{TE}}(x, y, z) + \vec{E}_{\text{TM}}(x, y, z) \\ &= \mathcal{F}^{-1}\{\vec{E}_{\text{TE}}(k_x, k_y, z)(-\hat{\mathbf{m}})\} \\ &\quad + \mathcal{F}^{-1}\{\vec{E}_{\text{TM}}(k_x, k_y, z)\hat{\mathbf{e}}\}\end{aligned}\quad (35)$$

where \vec{E}_{TE} and \vec{E}_{TM} are the spectral field of polarizations TE and TM, respectively, \mathcal{F}^{-1} denotes the inverse Fourier transform operator and the components \vec{E}_{TE} and \vec{E}_{TM} are the results of the inverse Fourier transform of the spectral electric field in TE and TM polarizations, respectively. The polarization vectors $\hat{\mathbf{m}}$ and $\hat{\mathbf{e}}$ associated with TE and TM modes have been defined in Section II, respectively.

Since the ground plane is located below the antenna, mainly downward waves are considered in this article, for which $|z - z'|$ can be written as $z' - z$ such that $\exp(-jk_z|z - z'|) = \exp(-jk_z z') \exp(jk_z z)$. The relation between the electric field and the vector potential is given by

$$\vec{E} = -jk\eta \left(\mathbb{I} + \frac{\nabla\nabla}{k^2} \right) \cdot \vec{A} \quad (36)$$

where \mathbb{I} is the unit dyad and \vec{A} is obtained by inserting (32) into (34) while swapping spatial and spectral integration. This provides a spectral representation for \vec{E} in which a given polarization p can be selected by projection on $\hat{\mathbf{e}}_p$ (defined in Section II)

$$\begin{aligned}\vec{E}_p &= -\frac{jk\eta}{(2\pi)^2} \iint_{-\infty}^{\infty} \hat{\mathbf{e}}_p \frac{e^{-j(k_x x + k_y y - k_z z)}}{2jk_z} \hat{\mathbf{e}}_p \cdot \left[\mathbb{I} - \frac{\vec{k}\vec{k}}{k^2} \right] \\ &\quad \cdot \vec{F}_b(k_x, k_y) dk_x dk_y\end{aligned}\quad (37)$$

with

$$\vec{F}_b(k_x, k_y) = \iiint_{V'} \vec{J}_b(\vec{r}') e^{j(k_x x' + k_y y' - k_z z')} dV'. \quad (38)$$

APPENDIX C

INFINITE INTEGRAL INVOLVING BESSEL FUNCTION

Let us consider a function $f(x)$, which is analytical except for some singularities, such that the poles of $f(x)J_n(x\rho)$ are simple poles not located on the positive real axis. If $f(x)$ is an odd function, then [38]

$$\int_0^{\infty} f(x) J_n(x\rho) x^n dx = j\pi \sum_q \text{Res}_q[f(x)H_n^{(2)}(x\rho) x^n] \quad (39)$$

where ρ is a real positive constant, $H_n^{(2)}$ is the second-type Hankel function of order n , and $\text{Res}_q[g(x)]$ defines the residue of the function g for a given pole q . If the function $f(x)$ is even [38]

$$\int_0^{\infty} f(x) J_n(x\rho) x^n dx = j\pi \sum_q \text{Res}_q[f(x)\mathcal{H}_n^+(x\rho) x^n] \quad (40)$$

where $\mathcal{H}_n^+(x)$ is a linear combination of an Anger function $\mathcal{J}_n(x)$ and a Weber function $E_n(x)$ [23, Sec.10.1]

$$\mathcal{H}_n^+(x) = \mathcal{J}_n(x) + jE_n(x). \quad (41)$$

The Anger function is identified to the Bessel function of the same order when n is a natural number, which is always the case here. Details regarding the series representation of the Weber functions are given below.

The Weber function [23, Sec.10.1], [34, Sec.8.58] is the solution of an inhomogeneous Bessel equation. Its integral form is defined as

$$E_n(z) = \int_0^{\pi} \sin(n\pi - z \sin \theta) d\theta. \quad (42)$$

The function can be written as the following expansion in ascending powers of z [34, Sec.8.581]:

$$\begin{aligned}E_n(z) &= \sin \frac{n\pi}{2} \sum_{m=0}^{\infty} \frac{(-1)^m \left(\frac{z}{2}\right)^{2m}}{\Gamma(m+1+\frac{n}{2}) \Gamma(m+1-\frac{n}{2})} \\ &\quad - \cos \frac{n\pi}{2} \sum_{m=0}^{\infty} \frac{(-1)^m \left(\frac{z}{2}\right)^{2m+1}}{\Gamma(m+\frac{3}{2}+\frac{n}{2}) \Gamma(m+\frac{3}{2}-\frac{n}{2})}.\end{aligned}\quad (43)$$

This formulation is sufficiently efficient around the origin, where it can be evaluated with few terms with high accuracy. To the contrary, when $|z| \gtrsim 10$ and $n \leq 5$, more than 15 terms are needed in (43) to obtain a relative error of 0.001. At this point, it is more efficient to use an asymptotic formulation of the function. In our approach, we need to evaluate the Weber function of odd order for arguments lying in the lower complex plane [see (22)]. The Weber function can be efficiently evaluated for large arguments lying in the upper plan as [23, Sec.10.13]

$$\begin{aligned}E_n(z) &= -Y_n(z) - \frac{1 + \cos n\pi}{\pi z} \\ &\quad \times \left[1 - \frac{(1^2 - n^2)}{z^2} + \frac{(1^2 - n^2)(3^2 - n^2)}{z^4} - \dots \right] \\ &\quad - \frac{1 - \cos n\pi}{\pi z} \left[\frac{n}{z} - \frac{n(2^2 - n^2)}{z^3} \right. \\ &\quad \left. + \frac{n(2^2 - n^2)(4^2 - n^2)}{z^5} - \dots \right]\end{aligned}\quad (44)$$

where $Y_n(z)$ is the second-type Bessel function. After inspecting (43), the following equation can be deduced for any odd order n :

$$\begin{aligned}E_n(z) &= E_n(-z) \\ &= E_n(ze^{j\pi})\end{aligned}\quad (45)$$

which means that the asymptotic form (44) can be used for negative imaginary z . With this formulation, when $|z| \gtrsim 10$ and $n \leq 5$, the Weber function can be evaluated with a relative error less than 0.001 using (44) with two terms of the infinite sum.

ACKNOWLEDGMENT

The authors would like to thank Dr. H. Pienaar and Dr. Q. Gueuning for providing the FEKO simulations that enabled the validation part of this article.

REFERENCES

- [1] *The Square Kilometer Array*. Accessed: May 2019. [Online]. Available: <https://www.skatelescope.org/>
- [2] E. de Lera Acedo, N. Razavi-Ghods, N. Troop, N. Drought, and A. J. Faulkner, "SKALA, a log-periodic array antenna for the SKA-low instrument: Design, simulations, tests and system considerations," *Experim. Astron.*, vol. 39, no. 3, pp. 567–594, 2015.
- [3] J. Cavillot, H. Bui-Van, C. Craeye, H. Pienaar, and E. de Lera Acedo, "Efficient analysis of a 3D antenna installed on a finite ground plane," in *Proc. Eur. Conf. Antennas Propag. (EuCAP)*, London, U.K., 2018, pp. 553–554.
- [4] N. A. Aboserwal, C. A. Balanis, and C. R. Birtcher, "Impact of finite ground plane edge diffraction on radiation patterns of aperture antennas," *Prog. Electromagn. Res. B*, vol. 55, pp. 1–21, 2013.
- [5] H. M. Ibrahim and D. T. Stephenson, "Radiation patterns of a $\lambda/4$ monopole mounted on thick finite square or circular ground plane," *Int. J. Electron.*, vol. 64, no. 3, pp. 345–358, Mar. 1988.
- [6] D. B. Davidson, *Computational Electromagnetics for RF and Microwave Engineering*. Cambridge, U.K.: Cambridge Univ. Press, 2011.
- [7] R. F. Harrington, *Field Computations by Moment Method in Electromagnetics*. Hoboken, NJ, USA: Wiley, 1993.
- [8] R. Coifman, V. Rokhlin, and S. Wandzura, "The fast multipole method for the wave equation: A pedestrian prescription," *IEEE Antennas Propag. Mag.*, vol. 35, no. 3, pp. 7–12, Jun. 1993.
- [9] J. M. Song and W. C. Chew, "Multilevel fast multipole algorithm for solving combined field integral equations of electromagnetic scattering," *Microw. Opt. Technol. Lett.*, vol. 10, pp. 14–19, Sep. 1995.
- [10] E. Suter and J. R. Mosig, "A subdomain multilevel approach for the efficient MoM analysis of large planar antennas," *Microw. Opt. Technol. Lett.*, vol. 26, no. 4, pp. 270–277, Aug. 2000.
- [11] V. V. S. Prakash and R. Mittra, "Characteristic basis function method: A new technique for efficient solution of method of moments matrix equations," *Microw. Opt. Technol. Lett.*, vol. 36, pp. 95–100, Jan. 2003.
- [12] L. Matekovits, V. A. Laza, and G. Vecchi, "Analysis of large complex structures with the synthetic-functions approach," *IEEE Trans. Antennas Propag.*, vol. 55, no. 9, pp. 2509–2521, Sep. 2007.
- [13] W. B. Lu, T. J. Cui, Z. G. Qian, X. X. Yin, and W. Hong, "Accurate analysis of large-scale periodic structures using an efficient subdomain basis function method," *IEEE Trans. Antennas Propag.*, vol. 52, no. 11, pp. 3078–3085, Nov. 2004.
- [14] X. Zhao, Z. Lin, Y. Zhang, S.-W. Ting, and T. K. Sarkar, "Parallel hybrid method of HOMoM-MLFMA for analysis of large antenna arrays on an electrically large platform," *IEEE Trans. Antennas Propag.*, vol. 64, no. 12, pp. 5501–5506, Dec. 2016.
- [15] E. Lucente, A. Monorchio, and R. Mittra, "An iteration-free MoM approach based on excitation independent characteristic basis functions for solving large multiscale electromagnetic scattering problems," *IEEE Trans. Antennas Propag.*, vol. 56, no. 4, pp. 999–1007, Apr. 2008.
- [16] L. Crocco, F. Cuomo, and T. Isernia, "Generalized scattering-matrix method for the analysis of two-dimensional photonic bandgap devices," *J. Opt. Soc. Amer. A, Opt. Image Sci.*, vol. 24, no. 10, pp. A12–A22, 2007.
- [17] J. Yeo, V. V. S. Prakash, and R. Mittra, "Efficient analysis of a class of microstrip antennas using the characteristic basis function method (CBFM)," *Microw. Opt. Technol. Lett.*, vol. 39, no. 6, pp. 456–464, 2003.
- [18] C. Craeye, "A fast impedance and pattern computation scheme for finite antenna arrays," *IEEE Trans. Antennas Propag.*, vol. 54, no. 10, pp. 3030–3034, Oct. 2006.
- [19] D. González-Ovejero, F. Mesa, and C. Craeye, "Accelerated macro basis functions analysis of finite printed antenna arrays through 2D and 3D fast multipoles," *IEEE Trans. Antennas Propag.*, vol. 61, no. 2, pp. 707–717, Feb. 2013.
- [20] D. Gonzalez-Ovejero and C. Craeye, "Interpolatory macro basis functions analysis of non-periodic arrays," *IEEE Trans. Antennas Propag.*, vol. 59, no. 8, pp. 3117–3122, Aug. 2011.
- [21] B. Hu, W. C. Chew, E. Michielssen, and J. Zhao, "Fast inhomogeneous plane wave algorithm for the fast analysis of two-dimensional scattering problems," *Radio Sci.*, vol. 34, no. 4, pp. 759–772, 1999.
- [22] V. I. Okhmatovski and A. C. Cangellaris, "A new technique for the derivation of closed-form electromagnetic Green's functions for unbounded planar layered media," *IEEE Trans. Antennas Propag.*, vol. 50, no. 7, pp. 1005–1016, Jul. 2002.
- [23] G. N. Watson, *Theory Bessel Functions*, 2nd ed. Cambridge, U.K.: Cambridge Univ. Press, 1966.
- [24] K. Alkhalifeh, G. Hislop, N. A. Ozdemir, and C. Craeye, "Efficient MoM simulation of 3-D antennas in the vicinity of the ground," *IEEE Trans. Antennas Propag.*, vol. 64, no. 12, pp. 5335–5344, Dec. 2016.
- [25] C. Craeye, J. Lavidia, R. Masskant, and R. Mittra, "Macro basis function framework for solving Maxwell's equations in surface integral equation form," *FERMAT J.*, vol. 3, pp. 1–16, 2014.
- [26] H. Bui-Van *et al.*, "Fast and accurate simulation technique for large irregular arrays," *IEEE Trans. Antennas Propag.*, vol. 66, no. 4, pp. 1805–1817, Apr. 2018.
- [27] S. Karki and C. Craeye, "Macro basis function interactions accelerated with the inhomogeneous plane waves," in *Proc. Int. Conf. Electromagn. Adv. Appl. (ICEAA)*, Sep. 2015, pp. 1314–1317.
- [28] Q. Gueuning, C. Craeye, and C. Oestges, "Sampling rules for an inhomogeneous plane-wave representation of scattered fields," *IEEE Trans. Antennas Propag.*, vol. 67, no. 3, pp. 1697–1708, Mar. 2018.
- [29] E. Martini, C. Craeye, N. Ozdemir, and S. Maci, "Harmonics-based inhomogeneous plane-wave method (HIPW)," *IEEE Trans. Antennas Propag.*, vol. 63, no. 5, pp. 2331–2336, May 2015.
- [30] H. Weyl, "Ausbreitung elektromagnetischer Wellen über einem ebenen Leiter," *Annalen Der Physik*, vol. 365, no. 21, pp. 481–500, Aug. 1919.
- [31] R. R. Boix, F. Mesa, and F. Medina, "Application of total least squares to the derivation of closed-form green's functions for planar layered media," *IEEE Trans. Microw. Theory Techn.*, vol. 55, no. 2, pp. 268–280, Feb. 2007.
- [32] S. N. Jha and C. Craeye, "Contour-FFT based spectral domain MBF analysis of large printed antenna arrays," *IEEE Trans. Antennas Propag.*, vol. 62, no. 11, pp. 5752–5764, Nov. 2014.
- [33] P. Crespo-Valero, M. Mattes, I. Stevanovic, and J. R. Mosig, "A numerically stable transmission line model for multilayered Green's functions," in *Proc. Antennas Propag. Soc. Int. Symp.*, Washington, DC, USA, vol. 3A, Jul. 2005, pp. 200–203.
- [34] I. S. Gradshteyn and I. M. Ryzhik, *Table of Integrals, Series, and Products*. New York, NY, USA: Academic, 2007.
- [35] B. Gustavsen and A. Semlyen, "Rational approximation of frequency domain responses by vector fitting," *IEEE Trans. Power Del.*, vol. 14, no. 3, pp. 1052–1061, Jul. 1999.
- [36] V. N. Kourkoulos and A. C. Cangellaris, "Accurate approximation of Green's functions in planar stratified media in terms of a finite sum of spherical and cylindrical waves," *IEEE Trans. Antennas Propag.*, vol. 54, no. 5, pp. 1568–1576, May 2006.
- [37] T. N. Kaifa, "Direct rational function fitting method for accurate evaluation of Sommerfeld integrals in stratified media," *IEEE Trans. Antennas Propag.*, vol. 60, no. 1, pp. 282–291, Jan. 2012.
- [38] Q.-G. Lin, "Infinite integrals involving Bessel functions by contour integration," *Integral Transforms Special Functions*, vol. 24, no. 10, pp. 783–795, Jan. 2013.
- [39] R. Vescovo, "Inversion of block-circulant matrices and circular array approach," *IEEE Trans. Antennas Propag.*, vol. 45, no. 10, pp. 1565–1567, Oct. 1997.
- [40] M. A. Carr, J. L. Volakis, and D. C. Ross, "Acceleration of free-space discrete body of revolution codes by exploiting circulant submatrices," *IEEE Trans. Antennas Propag.*, vol. 50, no. 9, pp. 1319–1322, Sep. 2002.
- [41] *Altair Com*. Accessed: May 2019. [Online]. Available: <https://www.altairhyperworks.com/product/FEKO/>
- [42] S. M. Rao, D. R. Wilton, and A. W. Glisson, "Electromagnetic scattering by surfaces of arbitrary shape," *IEEE Trans. Antennas Propag.*, vol. AP-30, no. 3, pp. 409–418, May 1982.
- [43] K. A. Michalski and J. R. Mosig, "Multilayered media Green's functions in integral equation formulations," *IEEE Trans. Antennas Propag.*, vol. 45, no. 3, pp. 508–519, Mar. 1997.
- [44] B. Mort, F. Dulwich, N. Razavi-Ghods, E. de Lera Acedo, and K. Grainge, "Analysing the impact of far-out sidelobes on the imaging performance of the SKA-LOW telescope," *Monthly Notices Roy. Astronomical Soc. (MNRAS)*, vol. 465, no. 3, pp. 3680–3692, Mar. 2017.
- [45] A. Ludwig, "The definition of cross polarization," *IEEE Trans. Antennas Propag.*, vol. AP-21, no. 1, pp. 116–119, Jan. 1973.
- [46] E. De Lera Acedo *et al.*, "SKA aperture array verification system: Electromagnetic modeling and beam pattern measurements using a micro UAV," *Exp. Astron.*, vol. 45, no. 1, pp. 1–20, Mar. 2018.
- [47] T. D. Carozzi and G. Woan, "A fundamental figure of merit for radio polarimeters," *IEEE Trans. Antennas Propag.*, vol. 59, no. 6, pp. 2058–2065, Jun. 2011.
- [48] Q.-H. Liu and W. C. Chew, "Applications of the conjugate gradient fast Fourier Hankel transfer method with an improved fast Hankel transform algorithm," *Radio Sci.*, vol. 29, pp. 1009–1022, Dec. 1994.

- [49] W. Cai and T. Yu, "Fast calculations of dyadic green's functions for electromagnetic scattering in a multilayered medium," *J. Comput. Phys.*, vol. 165, no. 1, pp. 1–21, Nov. 2000.
- [50] K. A. Michalski, "Extrapolation methods for Sommerfeld integral tails," *IEEE Trans. Antennas Propag.*, vol. 46, no. 10, pp. 1405–1418, Oct. 1998.
- [51] Y. L. Chow, J. J. Yang, D. G. Fang, and G. E. Howard, "A closed-form spatial Green's function for the thick microstrip substrate," *IEEE Trans. Microw. Theory Techn.*, vol. 39, no. 3, pp. 588–592, Mar. 1991.



Jean Cavillot (S'19) was born in Arlon, Belgium, in 1994. He received the bachelor's and master's degrees in electrical engineering from the Université catholique de Louvain (UCLouvain), Louvain-la-Neuve, Belgium, in 2015 and 2017, respectively. He is currently pursuing the Ph.D. degree with the Antenna Group, UCLouvain under FRIA Grant from Fonds National de la Recherche Scientifique (FNRS).

His topics of research interest include numerical methods for arrays installed on finite platform.



Denis Tihon (M'18) received the B.Eng. and M.Eng. degrees in physical engineering from the Université catholique de Louvain (UCLouvain), Louvain-la-Neuve, Belgium, in 2011 and 2013, respectively. He is currently pursuing the Ph.D. degree with the Institute of Information and Communication Technologies, Electronics and Applied Mathematics (ICTEAM) on the numerical modeling of periodic absorbers and partially coherent fields, in collaboration with the University of Cambridge, Cambridge, U.K.

Between 2013 and 2019, he was a Teaching Assistant with UCLouvain. Between 2017 and 2019, he also worked on the simulation of magnetic resonance imaging (MRI) antennas in the context of M-Cube FET-OPEN European Project. Since 2019, he has been holding a post-doctoral position, under the M. Skłodowska-Curie Fellowship, at the Cavendish Laboratory, Cambridge, where he was studying thermal emitters and partially coherent fields. His current research interests include the method of moments, the modeling of thermal and electroluminescent sources, and partially coherent fields.



Francisco Mesa (M'93–SM'11–F'14) received the Licenciado and Ph.D. degrees in physics from the Universidad de Sevilla, Seville, Spain, in 1989 and 1991, respectively.

He is currently a Professor with the Departamento de Física Aplicada I, Universidad de Sevilla. His current research interest includes electromagnetic propagation/radiation in planar structures.



Eloy de Lera Acedo received the Ph.D. degree from the University Carlos III of Madrid, Getafe, Spain, in 2010.

He is currently the PI and a Principal Research Associate with the Cavendish Astrophysics Group, where he has developed his career on 21 cm radio cosmology and instrumentation for radio astrophysics. He is also the PI of the REACH experiment, a project aiming to detect the 21 cm global signature signal from the Cosmic Dawn and the Epoch of Re-ionization. He leads the Cm-wave Radio Astronomy and Novel Sensors Research Group, Cavendish Astrophysics, Cambridge, U.K., and has led the Antenna and low noise amplifier (LNA) Work package (AL WP) of the Aperture Array Design Consortium, which he developed the array stations for the SKA1-LOW telescope. Within the AL WP, he has also led the design and development of SKALA, and the SKA Log periodic Antenna and its LNA. He has also led substantial pieces of work in other international projects such as the Hydrogen Epoch of Re-ionization Array (HERA) for which he has led the design of the wide band feed within the analog team group. His research interest ranges from ultra wideband array and antenna design, electromagnetic modeling, telescope calibration, and low-noise systems to the broader science case of 21 cm cosmology experiments.



Christophe Craeye (M'98–SM'11) was born in Belgium in 1971. He received the Electrical Engineering and B.Phil. degrees from the Université catholique de Louvain (UCL), Louvain-la-Neuve, Belgium, and the Ph.D. degree in applied sciences from UCL, in 1994 and 1998, respectively.

From 1994 to 1999, he was a Teaching Assistant with UCL and carried out research on the radar signature of the sea surface perturbed by rain, in collaboration with NASA and European Space Agency (ESA). From 1999 to 2001, he was a Post-Doctoral

Researcher with the Eindhoven University of Technology, Eindhoven, The Netherlands. He was with the University of Massachusetts, Amherst, MA, USA, in 1999. He was with the Netherlands Institute for Research in Astronomy, Dwingeloo, The Netherlands, in 2001. In 2002, he started an antenna research activity with UCL, where he is currently a Professor. He was with the Astrophysics and Detectors Group, University of Cambridge, Cambridge, U.K., in 2011. His research was funded by the Region Wallonne, European Commission, ESA, FNRS, and UCL. His current research interests include mutual coupling, finite antenna arrays, wideband antennas, small antennas, metamaterials, fast physical optics, and numerical methods for fields in periodic media, with applications to communication and sensing systems.

Dr. Craeye received the 2005–2008 Georges Vanderlinden Prize from the Belgian Royal Academy of Sciences in 2009. He was an Associate Editor of the *IEEE TRANSACTIONS ON ANTENNAS AND PROPAGATION* from 2004 to 2010 and for the *IEEE ANTENNAS AND WIRELESS PROPAGATION LETTERS* from 2011 to 2017.